EDGE ARTICLE

Check for updates

New light on the imbroglio surrounding the C8H6+ isomers formed from ionized azulene and naphthalene using ion–molecule reactions†

Corentin Rossi, [ID] [a] Giel Muller, [b] Roland Thissen, [cd] Claire Romanzin, [cd] Christian Alcaraz, [ID] [cd] Sandesh Gondarry, [e] Paul M. Mayer [ID] [e] and Ugo Jacovella [ID] *[a]

Most polycyclic aromatic hydrocarbons (PAHs) can isomerize with internal energies near to or below the dissociation threshold. The $C_{10}H_8^+$ group of ions, made up of the naphthalene (**Naph+**) and the azulene (**Azu+**) radical cations, is a prototypical example. $C_8H_6^+$ isomers are important species in the growth kinetics and formation of complex organic molecules, and more generally fragments from larger PAHs, yet information about $C_8H_6^+$ structures is scarce and contradictory. Here, ion–molecule reactions were carried out and the tunable photoionization chemical monitoring technique was used to probe the $C_8H_6^+$ isomers formed upon C_2H_2-loss from **Naph+** and **Azu+**. The experimental findings were interpreted with the support of *ab initio* and kinetics calculations. To facilitate the interpretation of these data, chemical reactivity starting from phenylacetylene (**PA**) was studied. It was found that most of the $C_8H_6^+$ ions formed from $C_{10}H_8$, in a timescale of 40 µs, are **PA+** in the vicinity of the dissociation threshold. No evidence of the pentalene radical cation (**PE+**) was observed and explanations to reconcile previous results are presented.

Introduction

Energetic gaseous polycyclic aromatic hydrocarbons (PAHs) react in environments spanning from plasmas, flames, planetary ionospheres, to stellar and interstellar regions.[1–8] The photoprocessing of gaseous PAHs leads to unimolecular reactions such as isomerization and dissociation, which often compete. The major dissociation channels of PAHs involve the loss of atomic or molecular hydrogen and C_2H_2, with dissociative ionization giving a quasi-balanced branching ratio for small PAHs such as naphthalene (**Naph**), and in favor of H/H2 loss as the PAH size increases.[9] The C_2H_2-loss reaction, in particular, plays a central role in stirring the composition of species formed in environments where energized PAHs can be found.

Better understanding of the unimolecular reactions of small prototypical PAH radical cations such as **Naph+** and **Azu+** is necessary to predict reactivities of larger PAHs and elucidate

aUniversité Paris-Saclay, CNRS, Institut des Sciences Moléculaires d'Orsay, 91405 Orsay, France. E-mail: ugo.jacovella@universite-paris-saclay.fr

bMolecular Horizons and School of Chemistry and Molecular Bioscience, University of Wollongong, Wollongong, New South Wales 2522, Australia
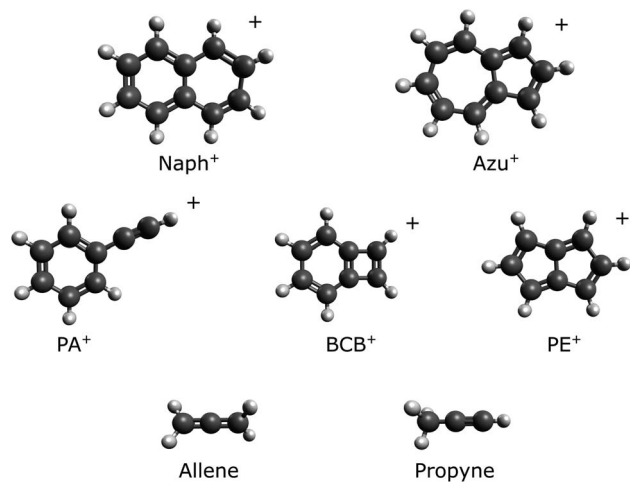
cUniversité Paris-Saclay, CNRS, Institut de Chimie Physique, UMR8000, 91405 Orsay, France

dSynchrotron SOLEIL, L'Orme des Merisiers, 91192 Saint Aubin, Gif-sur-Yvette, France

eDepartment of Chemistry and Biomolecular Sciences, University of Ottawa, Ottawa K1N 6N5, Canada

† Electronic supplementary information (ESI) available. See DOI: https://doi.org/10.1039/d3sc03015f

their relationship with carbon clusters.[10–12] The pioneering works on the fate of **Naph** and **Azu** were performed by the groups of Leach[13–16] and Lifshitz.[17–21] Through use of photoionization spectroscopy, time-resolved photodissociation spectroscopy, *ab initio* calculations, and Rice–Ramsperger–Kassel–Marcus (RRKM) calculations, these studies revealed H-loss and C_2H_2-loss as the two primary dissociation channels, occurring with equal branching ratios owing to their similar activation energies and dissociation rate constants. Furthermore, photoionization mass spectra of **Naph** and **Azu** have been shown to be similar at photon energy greater than 20 eV.

Structural information about the $C_8H_6^+$ fragment of **Naph+** and **Azu+** has been scattered and continually evolving over the last three decades. The structures of the molecular ions of interest are provided in Scheme 1. In the early 1990s, Leach and coworkers proposed the formation of the phenylacetylene radical cation (**PA+**) as the primary structure resulting from dissociative photoionization (within a few tens of µs).[14] They confirmed this proposition one year later by conducting similar experiments with deuterated species.[15] In the same year, the Lifshitz group further supported the hypothesis that **PA+** is the major product resulting from ionized **Naph** and **Azu**, using time-resolved photoionization mass spectrometry (TPIMS), allowing the ions to evolve for 40 µs to 400 ms.[17] In the same study, they also corroborated this finding through collision activation (CA) spectra.

The cards were reshuffled in 1995 with the theoretical work of Granucci *et al.*,[22] which involved structure optimizations for

Scheme 1 Structures of the molecular ions and neutral targets of interest for this study.

$C_8H_6^+$ using Møller–Plesset perturbation theory (MP2) and the complete active space self-consistent field (CASSCF) method for energy calculations. The structures they considered included **PA⁺**, benzocyclobutadiene radical cation (**BCB⁺**), and the benzocyclopropenemethylene radical cation. The latter structure was discarded due to its significantly higher energy, but **BCB⁺** was found to be more stable than **PA⁺**. Two years later, Lifshitz and coworkers theoretically confirmed, using a coupled cluster method (CCSD(T)), that **BCB⁺** was the most stable structure among the three considered by Granucci *et al.*[22] The dissociation limit into $C_8H_6^+$ (**BCB⁺**) + C_2H_2 was then adopted as the lowest one in subsequent works by the Lifshitz group.[20,21]

In 1999, the Schwarz group employed a variety of complementary mass spectrometric techniques to confirm the structure of the $C_8H_6^+$ species formed from **Naph⁺**.[23] They expanded the range of possible structures to include acyclic, eight-membered ring, and were the first to consider the pentalene radical cation (**PE⁺**). Acyclic and eight-membered ring structures were considered unlikely products. **BCB⁺** was proposed as the most probable structure, mainly based on charge reversal (CR) experiments (30 μs timescale and ions formed by electron impact), in agreement with the previous theoretical work.[19,22] A couple of years later, van der Hart used density-functional theory (DFT) to study the most probable $C_8H_6^+$ structures formed from **Naph⁺**, concluding that both **BCB⁺** and **PA⁺** should be observable in photodissociation experiments.[24]

A major step forward came from the theoretical work of Mebel and coworkers, who mapped out the potential energy surface of $C_{10}H_8^+$ using the G3(MP2,CC)//B3LYP method.[25] They then performed RRKM and microcanonical variational state theory calculations to investigate the possible photodissociation mechanisms of **Azu⁺** at different photon energies.[25] They also computed the relative branching ratios of $C_8H_6^+$ structures obtained after C_2H_2 elimination using the steady-state approach. These branching ratios indicate that below 5.2 eV of internal energy in **Azu⁺**, **PA⁺** is the prevailing $C_8H_6^+$ structure but gets supplanted by **PE⁺** at internal energies greater than 5.2 eV above the **Azu⁺** ionization energy. The contribution of

BCB⁺, although marginal, increases with the internal energy. It is important to note that the total photon energy was assumed to be transferred into internal energy of the ion, neglecting Franck–Condon considerations and any radiative relaxation processes.

Solano and Mayer conducted similar work for **Naph⁺** but used a potential energy surface computed at a lower level of theory (UB3LYP/6-311+G(3df,2p)//UB3LYP/6-31G(d)), and found that **PA⁺** only becomes the major isomer when **Naph⁺** has more than 7.6 eV of internal energy.[26] Discrepancies between the results of kinetic calculations and those of Mebel group[25] may be due to the fact that kinetic modeling did not fully follow the master equation approach, included simplifying assumptions, and the initial internal energy distribution was different.

The dissociation pathway from $C_{10}H_8^+$ leading to **PE⁺** was experimentally evidenced for the first time by recording the infrared spectroscopic fingerprint of **PE⁺**.[27] $C_8H_6^+$ ions were generated by multiphoton dissociative ionization from **Naph** and were allowed to evolve for 200 ms before being ejected from the trap, which could be considered as equilibrium for a molecular system of this size. Other experiments on nitrogen-containing PAHs and larger PAHs then suggested a general trend for the formation of pentagons in the ionic species through the destruction of PAHs containing pure hexagonal geometries.[28,29] These mechanisms may help to rationalize the formation of fullerenes from larger energized PAHs[10,11]

Bull and coworkers[30] obtained similar results to Mebel and coworkers[25] using a coupled master equation combined with high-level potential energy surface calculations (CCSD(T)/cc-pVTZ).[30] At around 5.1 eV of internal energy in **Azu⁺** and **Naph⁺**, they calculated a ratio of 3/4 of $C_8H_6^+$ being **PA⁺** and 1/4 being **PE⁺** at equilibrium. This confirms that **PA⁺** is the dominant one at low internal energy before giving way to **PE⁺**, which should dominate the $C_8H_6^+$ population above its thermodynamic formation threshold, provided sufficient time is granted.

The present study focuses on the reactivity of $C_8H_6^+$ structures with **allene** and **propyne**, where the $C_8H_6^+$ structures are generated either by direct photoionization of phenylacetylene (**PA**) or dissociative photoionization of **Naph** and **Azu** molecules. We employ the tunable photoionization chemical monitoring technique,[31] an approach that has been successful in elucidating the structures of ionic fragments from dissociative ionization[32] and uncovering isomerization pathways.[33] The data set obtained from the current study provides chemical reference for one of the expected $C_8H_6^+$ species, specifically **PA⁺**, facilitating the data interpretation from dissociative ionization of $C_{10}H_8$ species. The experimental data are complemented by *ab initio* and kinetics calculations. Finally, results from former experimental works are discussed in the light of the present results and new interpretations are proposed to reconcile all the results.

Methods

Experimental

Parent ions were produced through photoionization using light over the 7.2 to 20 eV photon energy range using the DESIRS

undulator-based vacuum ultraviolet (VUV) beamline[34] at the SOLEIL synchrotron facility in Saint-Aubin (France). The temperature of the neutral precursors when irradiated by the VUV light was approximately 300 K. Higher-order light was removed from the beam using a gas filter filled with either Kr or Ne depending on the energy range. The reaction products were monitored using the CERISES apparatus consisting of a tandem mass spectrometer (quadrupole–octopole–octopole–quadrupole) coupled to a photoionization source.[35] Parent ions produced in the source were mass filtered by the first quadrupole and then guided by an octopole to the reaction cell while defining the collision energy. The ionic products of reactions were then radially confined and directed into the second quadruple mass filter. The absolute reaction cross sections were obtained by measuring the absolute pressure of the neutral reactant in the reaction cell and the parent and product ion counts. Measurements were taken across the photon energy range while the collision energy was fixed at 0.11 eV in the center-of-mass frame. The neutral reactants were introduced into the reaction cell at a low pressure (typically below 70 nbar) to ensure the attenuation of parent ion signal was less than 10%, providing a single-collision regime.

Computational

Stationary points on the ground state $C_8H_6^+$ potential energy surface around PA^+ were found by conducting relaxed potential energy surface scans of $C_8H_6^+$ structures along various internal degrees of freedom at the ωB97X-D/aug-cc-pVTZ level of theory using the Gaussian 16 software package.[36] The optimized geometry for each saddle point was verified by its single negative vibrational frequency and by intrinsic reaction coordinate (IRC) calculations.

Rice–Ramsperger–Kassel–Marcus (RRKM) theory was employed to calculate the $k(E)$ for relevant reactions according to the equation:[37]

$$k(E) = (\sigma N^{\ddagger}(E - E_0))/(h\rho(E)), \tag{1}$$

where σ is the reaction degeneracy, h is Planck's constant, $N^{\ddagger}(E - E_0)$ is the number of internal states for the transition state at an internal energy $E - E_0$ and $\rho(E)$ is the density of states for the reactant ion at internal energy E, calculated with the Beyer and Swinehart direct count algorithm.[38,39]

Results and discussions

Fig. 1 and 5 show reaction cross sections for the products of $C_8H_6^+$ ions, formed from **PA** (Fig. 1), **Naph**, and **Azu** (Fig. 5), reacting with **propyne** and **allene**. The cross sections are given as a function of photon energy. Below, we will first present results of reactions carried out using the **PA** precursor and then analyze the results with the support of *ab initio* calculations and RRKM modeling. Later, a similar scheme is followed for reactions of $C_8H_6^+$ produced from **Naph** and **Azu**.

$C_8H_6^+$ from PA

Observations. The reaction cross sections of $C_8H_6^+$ produced by direct photoionization of **PA** reacting with **propyne** and **allene** are presented in the left and right panels of Fig. 1, respectively. Only reaction channels leading to formation of
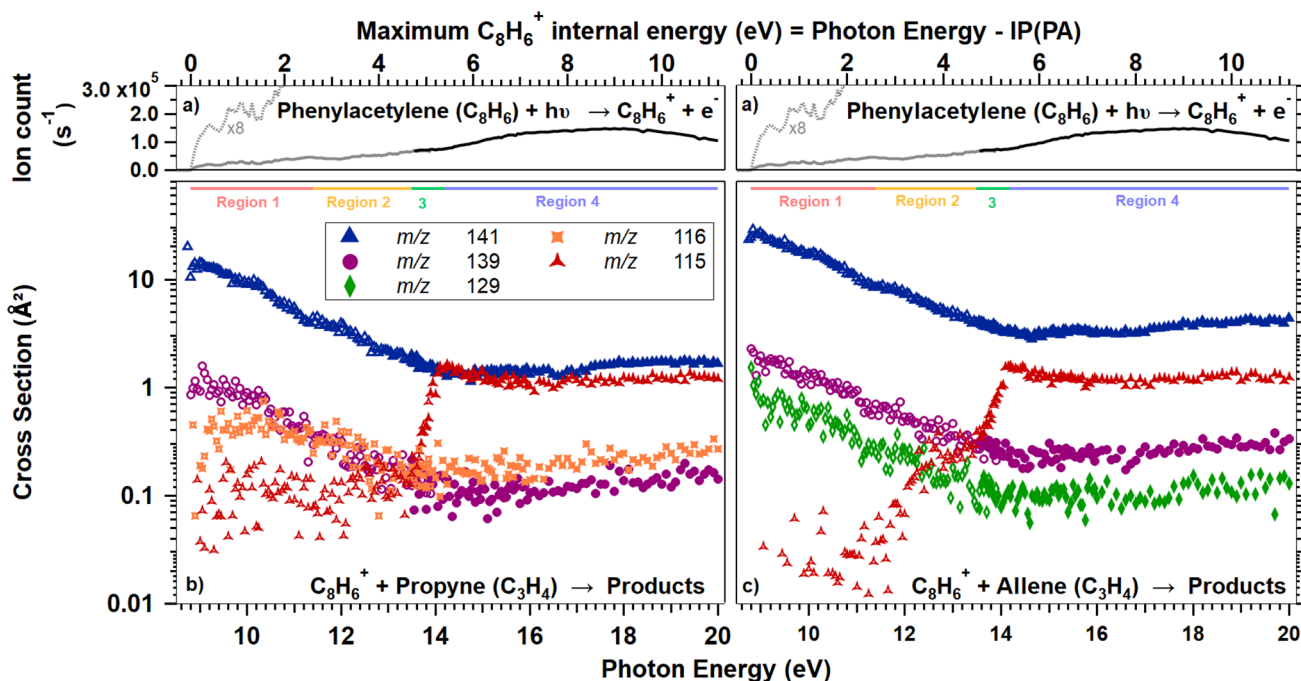

Fig. 1 The top panels (black traces) display the $C_8H_6^+$ photoion yield starting from phenylacetylene precursor (gray region was recorded with Kr in gas filter while dark region was recorded with Ne in gas filter). Bottom panels are reaction cross sections for the products resulting from $C_8H_6^+$ produced from phenyacetylene reacting, with (left) **propyne** and (right) **allene** as a function of photon energy.

products with cross section greater than 0.1 Å² are presented. The data indicate distinct reactivity behaviors across the 8.8–11.4 eV, 11.4–13.5 eV, 13.5–14.2 eV, and 14.2–20 eV energy regions. For simplicity, these regions will be referred to as regions 1, 2, 3 and 4, in order of increasing energy. The behavior of all observed reaction channels in each region is described below.

Reactions with Propyne

m/z **141;** *m/z* **139.** *m/z* 141 and *m/z* 139 channels correspond to the formation of $C_{11}H_9^+ + H$ and $C_{11}H_7^+ + H_2 + H$, respectively. These two channels show the same behavior with almost monotonic decreases in cross section, from 10 and 1 Å² to 2 and 0.1 Å², respectively, over the three lowest-energy regions. They reach a quasi-plateau in region 4 with weak growth in reactivity as the energy increases.

m/z **115.** The *m/z* 115 channel corresponds to formation of $C_9H_7^+ + [2C, 3H]$. The composition of the neutral product(s) cannot be directly retrieved from the experimental data, some possibilities include C_2H_3 and $C_2H_2 + H$. Regions 1 and 2 exhibit weak reactivity (≈ 0.1 Å²). The reactivity increases rapidly in the region 3 to reach nearly 2 Å² and plateaus slightly above 1 Å² in the region 4.

m/z **116.** The *m/z* 116 channel is consistent with the formation of $C_9H_8^+ + C_2H_2$. The reaction cross section is constant around 0.5 Å² in the region 1 before monotonically decreasing to 0.1 Å² at the end of the region 3. The reactivity is similar to the *m/z* 141 and *m/z* 139 channel in the fourth-energy region.

Reactions with Allene

m/z **141;** *m/z* **139.** These two reaction channels are similar to those resulting from reaction with **propyne**, but exhibit larger cross sections, by a factor 2.

m/z **115.** The *m/z* 115 yield from $C_8H_6^+$ reaction with **allene** is similar to that of the reaction with **propyne** over regions 1, 3, and 4. However, there is a notable difference in behavior in region 2, with a marked growth of *m/z* 115 products observed from the reaction with **allene** compared to negligible growth of the products resulting from the reaction with **propyne**.

m/z **129.** The reaction channel *m/z* 129 corresponds to $C_{10}H_9^+ + CH$ and follows the same trend as *m/z* 141 and *m/z* 139. This channel is not reported with **propyne** as it did not meet the 0.1 Å² reactivity criterion.

m/z **116.** Data for this channel were not recorded for this reactant.

Discussion

Region 1. As the ionisation energy (IE) of **PA** is 8.8 eV,[40] **PA**⁺ can be formed in region 1 (8.8–11.4 eV) with a maximal internal energy amount of 2.6 eV. The results of our calculations of the $C_8H_6^+$ potential energy surface (PES) are schematically represented in Fig. 2, and Table 1 lists the energies of minima and transition states (TSs) on the $C_8H_6^+$ PES. From Fig. 2 and Table 1, one can see that the lowest energy barrier to isomerize from **PA**⁺

Table 1 Energies of local minima and of transition states (TSs) of $C_8H_6^+$ species located on the PES presented in Fig. 2

Minima	Energies/eV	TSs	Energies/eV
PA⁺	0.00	PA⁺-1⁺	2.56
BCB⁺	−0.20	PA⁺-2⁺	2.57
PE⁺	−0.60	PA⁺-3⁺	2.64
1⁺	1.89	PA⁺-4⁺	2.61
2⁺	1.93	PA⁺-8⁺	2.88
3⁺	2.22	PA⁺-10⁺	3.26
4⁺	2.19	1⁺-6⁺	2.86
5⁺	0.62	2⁺-5⁺	3.08
6⁺	0.85	2⁺-7⁺	2.75
7⁺	2.60	3⁺-5⁺	3.19
8⁺	2.60	4⁺-6⁺	3.13
9⁺	2.62	7⁺-8⁺	3.13
10⁺	1.18	7⁺-9⁺	3.41
11⁺	1.87	8⁺-10⁺	3.49
12⁺	2.01	9⁺-11⁺	3.15
13⁺	0.66	10⁺-12⁺	2.86
14⁺	0.90	10⁺-13⁺	1.94
		10⁺-14⁺	2.75
		11⁺-BCB⁺	1.96
		12⁺-BCB⁺	2.42
		BCB⁺-PE⁺	2.57

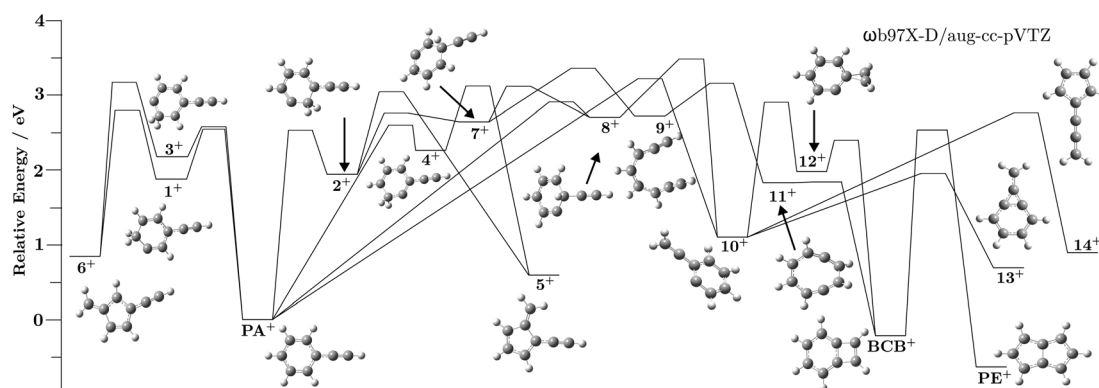**Fig. 2** $C_8H_6^+$ potential energy surface calculated at ωB97X-D/aug-cc-pVTZ level of theory.

is 2.56 eV and therefore we can consider that only the **PA**$^+$ structure is formed in region 1.

Region 2. The second region covers the photon energy from 11.4 to 13.5 eV, allowing for a maximum **PA**$^+$ internal energy of 4.7 eV. This region was identified through marked increase of the channel at m/z 115 in the reaction with **allene**. This reactivity change suggests either the formation of another $C_8H_6^+$ isomer(s) or that an endothermic barrier of reaction is overcome. RRKM calculations of four isomers (**1**$^+$, **2**$^+$, **3**$^+$, and **4**$^+$) were performed to assess their likelihood of formation in region 2. The resulting fractional abundances as a function of **PA**$^+$ internal energy are represented in the gray shaded zone in Fig. 3 and suggest that isomers **1**$^+$ and **2**$^+$ are the most likely ones to be formed in region 2. The isomers **1**$^+$ and **2**$^+$ are formed by a sigmatropic rearrangement, where a hydrogen atom in the *meta* position relative to the acetylenic group moves to the *para* and *ortho* positions, respectively. Nevertheless, their formation rates will remain too low to build up a large enough population to account for a reactivity change. As electronically excited states of **PA**$^+$ do not live long enough to reach the reaction cell (80 μs), only one possibility remains, which is the opening of an endothermic channel of **PA**$^+$ with **allene**. In these conditions, the RRKM calculations can thus serve as a guide for predicting the most probable $C_8H_6^+$ reactive structure to expect in the adduct formed with **allene**. Note that the reaction leading out of the **PA**$^+$ well to **BCB**$^+$ and **PE**$^+$ has a rate constant that is several orders of magnitude lower than the interconversion of **PA**$^+$ and isomers **1-4**$^+$ (see Fig. S7 in the ESI†).

Using this concept, we can investigate the contrasted unreactive behavior with **propyne** to provide an explanation. Fig. 4 presents possible entrance channels and adducts for the reactions of **1**$^+$ and **2**$^+$ with **propyne** and **allene**. The minimum reaction energy paths (MREPs) were calculated at the ωB97X-D/aug-cc-pVTZ level of theory and show that the reactions of **1**$^+$ and **2**$^+$ with **allene** are strongly exothermic, while those with **propyne** are either endothermic or thermoneutral. Interestingly, this difference in chemistry is rooted in the **propyne**/**allene** structures, leading to an easy H atom transfer through a four member intermediate in **allene**, impossible in the case of **propyne**, resulting in a much more stable structure when C_2H_3 is lost. Note that the loss of C_2H_3 compared to C_2H_2 + H is thermodynamically favored.

Region 3. Definitive elucidation of the isomer(s) formed in region 3 (13.5–14.2 eV, corresponding to a maximum of internal energy of 5.4 eV) is complicated by the large number of isomers that can be accessed at those energies. However, attention is drawn to the fact that the channel forming m/z 115 with **propyne** shows a steep increase and superimposes with the same channel with **allene**; none of the other channels are affected. One hypothesis is that the m/z 115 channel is extremely sensitive to the formation of one or a family of isomers. One family of isomers whose formation in small PAHs generally requires 4 to 6 eV of internal energy to be observable is that of species where the ring has been opened. One can notice that one of the highest barriers in the PES (Fig. 2) is the one leading to an open structure (**9**$^+$). This isomer is produced from **2**$^+$, through symmetric opening of the **7**$^+$ structure. Similar to region 2, the population transfer to **9**$^+$ is too small to explain the strong rise in the m/z 115 signal. However, it might suggest the formation of an adduct with a $C_8H_6^+$ structure resembling **9**$^+$. The formation of a m/z 115 product was previously observed in the reaction of m/z 76 (which was a fragment of **PA**$^+$) with **allene** and **propyne**.[41] This reaction was found to be very efficient (>10 Å^2) when $C_6H_4^+$ was generated with high internal energy (above
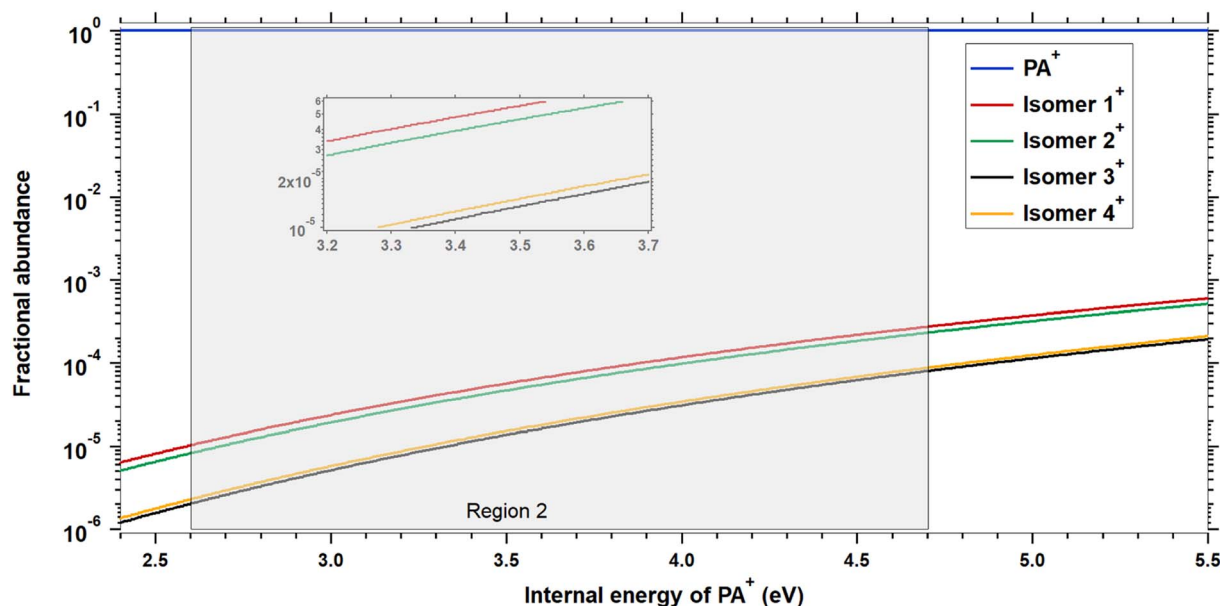

Fig. 3 Fractional abundances of **PA**$^+$ and **1**$^+$–**4**$^+$ as a function of the internal energy of **PA**$^+$. The shaded grey area represents the energies accessible in region 2. Note that these relative populations do not include the reactions out of the PA/1–4 ion well and thus do not reflect the true distribution of structures from Fig. 2.
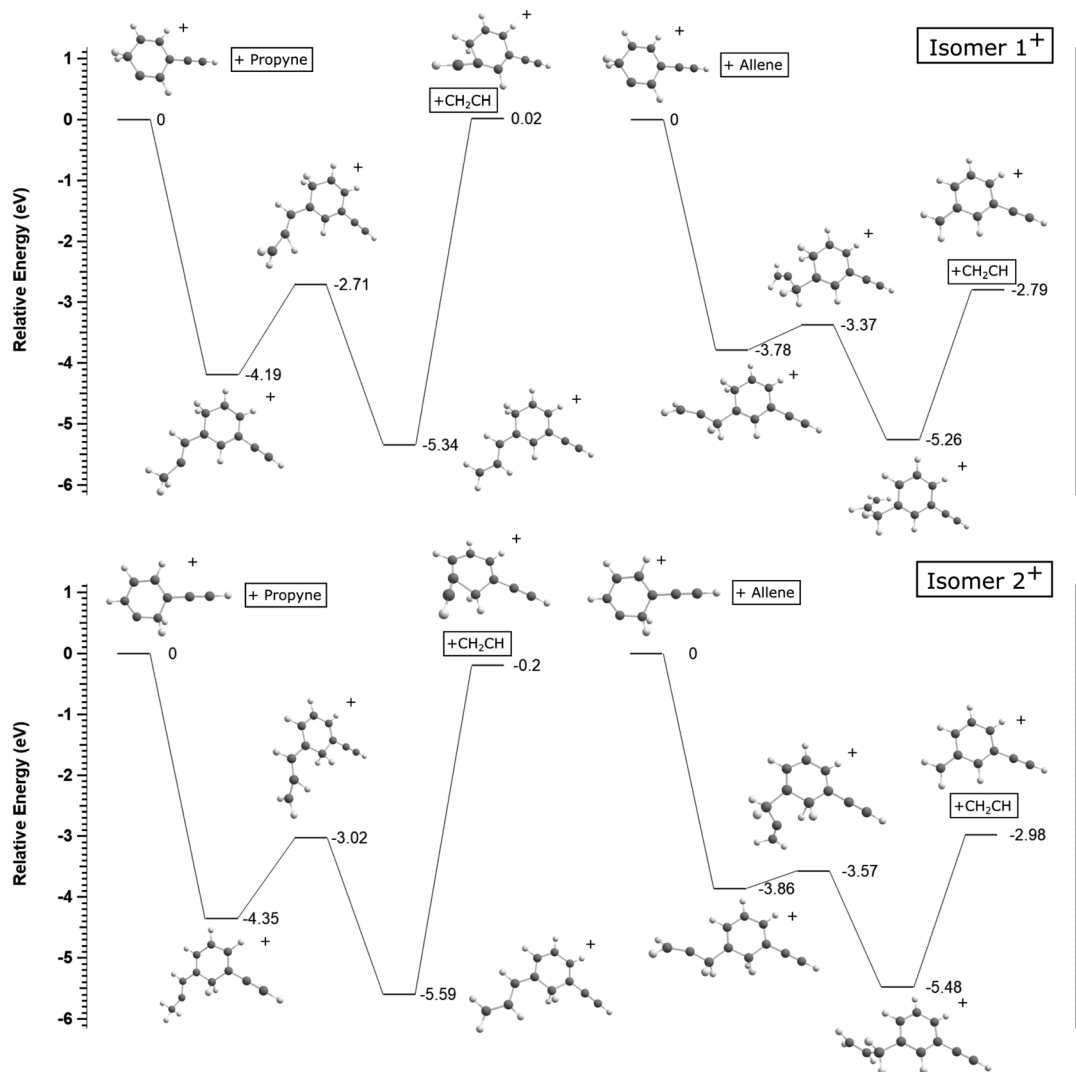
Fig. 4 Minimum reaction energy paths of isomers 1^+ (top panel) and 2^+ (bottom panel) with (left) **propyne** and (right) **allene**, leading to m/z 115 + C_2H_3. All calculations were done at the ωB97X-D/aug-cc-pVTZ level of theory.

14 eV, photon energy, where the ring opening was invoked to explain the change in reactivity). However, it seems very unlikely that the product observed in region 3, with a cross section of 1 Å^2, is the result of the sole metastable m/z 76 species formed in the region between the exit of the first quadrupole mass filter and the reaction cell. Nevertheless, the alternative scenario involving the reaction complex is again plausible, the highly excited $C_8H_6^+$ formed in region 3 may (in the reaction complex) transform into the highly excited $C_6H_4^+$ structure, leading to the same m/z 115 product. This transformation would result in the production of neutral products C_2H_2 and H, contrasting with the outcomes observed in region 2.

Region 4. The number of possible isomers that can be generated in region 4 (14.2–20 eV) is considerable. The data indicates that 5.4 eV above the IE of **PA** (corresponding to the beginning of region 4), the isomeric population of $C_8H_6^+$ reaches some sort of equilibrium, resulting in almost constant cross section for all reaction product channels (Fig. 1). Note that the ion yield for parent ion $C_8H_6^+$ exhibits a marked increase at

14.2 eV, indicating the presence of an excited state with large Franck–Condon factors (confirmed in the He I photoelectron spectrum).[42] This plateau in the chemical behavior hints at the fact that additional internal energy can no longer be absorbed by the $C_8H_6^+$ system. Two hypotheses can be considered to explain this. Either dissociative ionization occurs for all species produced with internal energies corresponding to region 4, or there is efficient fluorescence from the new electronic state.

$C_8H_6^+$ from Naph and Azu

The reaction cross sections of $C_8H_6^+$, produced by dissociative ionization of **Naph** and **Azu** and subsequent reaction with either **propyne** or **allene**, can be seen in the panels of Fig. 5. Only reaction channels leading to the formation of products with reaction cross sections greater than 0.1 Å^2 are presented. Only two channels meet this criterion, m/z 115 and 141, also observed with **PA**. The channels at m/z 116, 129, and 139 were not observed or had reaction cross-section below 0.1 Å^2.
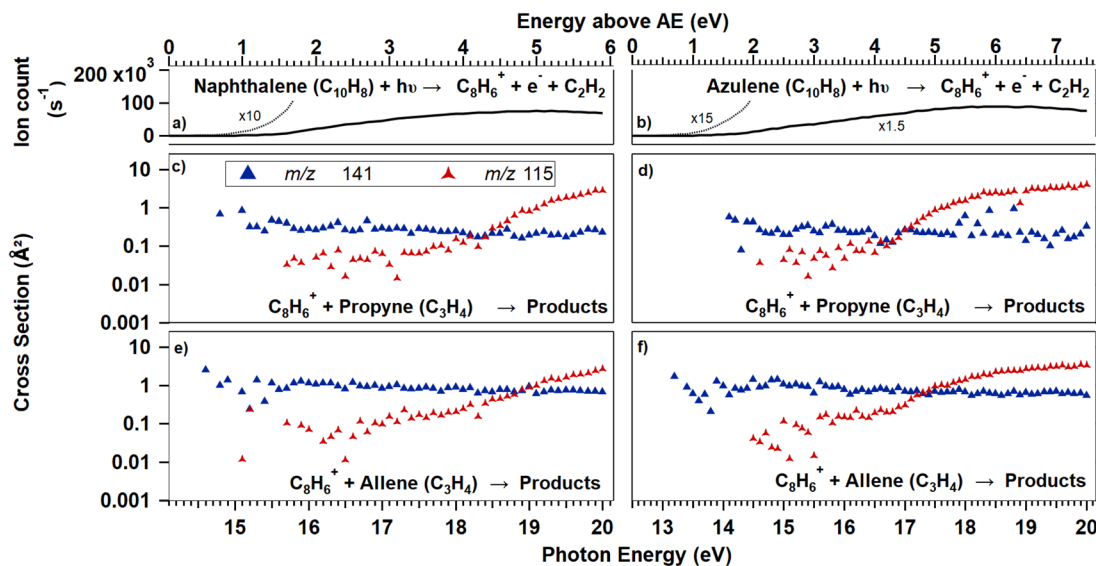
Fig. 5 The top panels (black traces), (a and b), display the $C_8H_6^+$ photoion yield starting from **Naph** and **Azu** precursors, respectively. Middle panels, (c and d), are reaction cross sections of $C_8H_6^+$ with **propyne** as a function of photon energy starting with **Naph** and **Azu** as precursors, respectively. Bottom panels, (e and f), are the reaction cross sections with **allene** from **Naph** and from **Azu**), respectively. We defined the AE as the photon energy where more than 20 $C_8H_6^+$ ions/s are detected.

Observations

It is striking that there is no isomeric effect, as the data appear to be identical for **Naph** and **Azu**, when corrected by their respective appearance energies, as clearly shown by Fig. 6 below. Similarly to previous studies,[14,17] the $C_8H_6^+$ threshold is very elusive, we therefore defined the AE as the photon energy where more than 20 $C_8H_6^+$ ions/s are detected.

m/z **141.** This channel is the most prominent at low internal energy – although it is relatively weak (around 1 Å^2). The reactivity is slightly greater with **allene** than with **propyne** (similarly to what is seen for **PA**$^+$) and, as mentioned, does not depend on the precursor used to generate $C_8H_6^+$. The reactivity shows

a constant decrease as the photon energy increases, reducing by a factor of 2 upon reaching 20 eV.

m/z **115.** The *m/z* 115 channel exhibits identical behavior to that observed when using **PA** as precursor. The shape of the reaction cross-section of *m/z* 115 for the reaction with **allene** and **propyne** indicates, similarly as when starting with **PA**, endothermic reactions and an onset at lower energy with **allene** compared to **propyne**.

Discussion

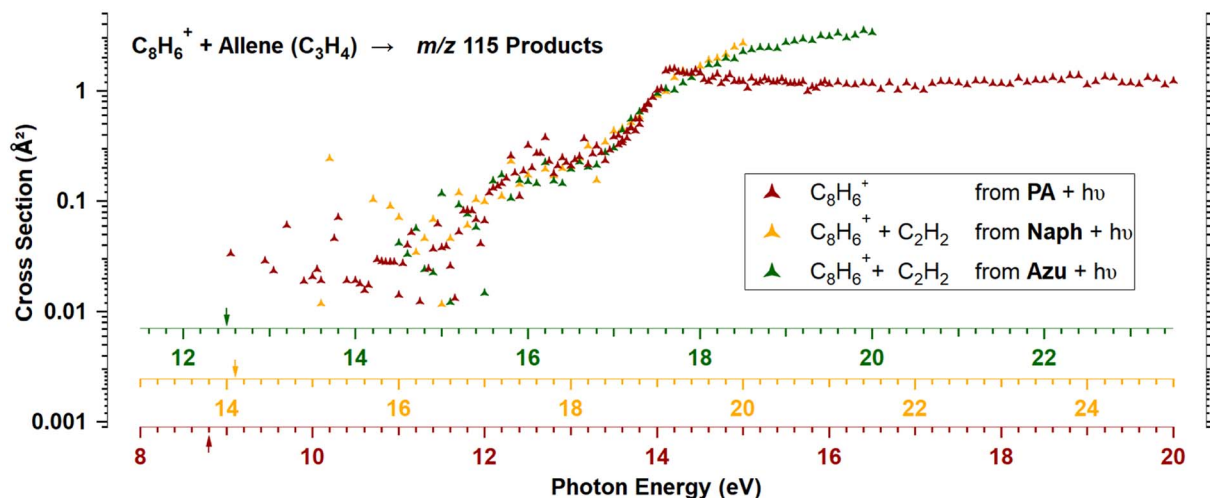Experimental and theoretical studies have disputed the isomeric structures of the major $C_8H_6^+$ fragment formed upon

Fig. 6 Reaction cross sections of $C_8H_6^+$ reacting with **allene** to produce ions with *m/z* 115 when $C_8H_6^+$ are formed from **PA** (red), **Naph** (orange), and **Azu** (green). The energy axes have been individually shifted to superimpose together. The arrows represent the IE of **PA** and the AEs of $C_8H_6^+$ from **Naph** (14.1 eV) and **Azu** (12.5 eV) precursors.

C_2H_2-loss but the most recent ones agree that **Azu**⁺ should fragment into **PE**⁺, while **Naph**⁺ should fragment into **PA**⁺ and **BCB**⁺. Typically starting either from **Azu**⁺ or **Naph**⁺, it was found that it requires $\approx$ 5 eV of internal energy for $C_{10}H_8^+$ systems to produce **PE**⁺ as the main fragment, which underlies the importance of the isomerization kinetics of the $C_{10}H_8^+$ ions. In our apparatus, when considering dissociative photoionization, only unimolecular dissociation reactions occurring faster than 40 μs can be probed. This is the time for ions to reach the entrance of the first mass filter. We have shown in a previous study considering a similar ionization energy range that within a timescale of 80 μs, only the isomerization from **Azu**⁺ to **Naph**⁺ is observed.[33] This observation is therefore not in favor of the formation of **PE**⁺ in our instrument. According to the calculations of Mebel and coworkers[25] (specifically Fig. 16 of ref. 25) and Bull and coworkers,[30] one could expect to have only **PA**⁺ formed in the vicinity of the $C_8H_6^+$ appearance energies of **Naph** and **Azu** at equilibrium. It is crucial to emphasize that in these calculations, it is considered that the entire population has a well defined internal energy value. However, when ions are prepared by photoionization, their internal energy varies between 0 and the photon energy minus IE or AE, depending on whether we consider **PA** or **Naph**/**Azu**, respectively. Consequently, this implies that the calculations provide an upper limit for the population transfer from **PA**⁺ to **PE**⁺.

Fig. 6 shows the reaction cross sections of m/z 115 with the three different precursors. The 3 datasets are only shifted in energy to be superimposed. This leads to values of $C_8H_6^+$ AEs from **Naph** and **Azu** precursors, and IE of **PA** to coincide within 0.3 eV. Although it is not a surprise that the reaction cross sections from **Naph** and **Azu** are similar, the reaction cross section from **PA** also overlays perfectly. This a decisive observable that indicates that **PA**⁺ is the reactive species at all photon energies up to the start of region 4 upon direct ionization of **PA** or dissociative ionization of **Naph** and **Azu** near dissociation thresholds. This result is a strong support for our hypothesis that close to 100% of **PA**⁺ is formed by dissociative ionization (for a timescale shorter than 40 μs), whatever the precursor but also informs that all internal energy is conserved by the ionic fragment when **PA**⁺ is formed by C_2H_2 elimination from **Naph** and **Azu**. This low kinetic energy release has been observed previously in a similar system, the *n*-butyl-benzene cation ($C_{10}H_{14}$) upon loss of C_3H_6, and was explained by the fact that the rate-limiting step is the isomerization reaction, prior to dissociation.[43]

In the energy range that would correspond to region 4 for the 3 precursors, it is disconcerting that, although the reaction cross sections are perfectly superimposed at lower energies, the cross section of m/z 115 becomes more important from **Naph** and **Azu** compared to **PA**. An explanation for this different behavior would relate to the previous observation that a strong increase of parent ion yield is observed for **PA**, at the energy corresponding to region 4, while such increase is absent in $C_8H_6^+$ yield from **Naph** and **Azu** (Fig. 5). The departure from similarity in the m/z 115 channel would indicate that the electronic state of **PA**⁺ efficiently dissociates and/or fluoresces and this state is efficiently populated by direct photoionization and not by dissociative ionization.

Another aspect that differentiate ions produced by direct ionization or dissociative photoionization is visible in the measured cross section for m/z 141. In Fig. 1, the fact that the channel m/z 141 continuously decreases (as do the channels m/z 116 and 129) indicates that these channels correspond to reaction mechanism where a complex (adduct) is formed. Such process is strongly increasing when energy is reduced. This was verified by conducted studies of the influence of the collision energy (see ESI†), with a rapid increase of cross-section when collision energy is decreased, faster than the Langevin trend. Similarly to collision energy, when considering photon energy, the channel of reaction from **PA** has a cross section of 10 Å² at photoionization threshold, and decreases to roughly 1 Å² when photon energy increase. When $C_8H_6^+$ is produced by dissociative photoionization from **Naph** and **Azu**, a maximum cross section of roughly 1 Å² is measured and decreases with photon energy. This discrepancy in numbers (apparent lack of 90% of the reaction cross section) is somewhat antagonist with the previous conclusion of 100% **PA**⁺ in all the $C_8H_6^+$ handled in our experiment, whatever the precursor. To reconcile these, one should consider that our experiments are performed without coincidence with energy-selected electrons. This implies that the ion population receives incremental amount of species in excited states as the photon energy increases, and this increment comes in addition to other states with less internal energy, depending on the Franck–Condon parameters leading to the states and the evolution of their relative cross section with photon energy. A more detailed discussion of this effect can be found in ref. 31. It is known that the Franck–Condon factor of the photoionizing origin band of **PA** is very strong as can be seen in the sharp threshold behavior of **PA**⁺ ion in Fig. 1 and in photoelectron spectra, for instance in ref. 42. This will efficiently produce **PA**⁺ with very limited internal energy by direct photoionization, which we can expect to exhibit a strong propensity to generate long-lived intermediate and exhibit sizable cross section for m/z 141 production. In contrast, the population of $C_8H_6^+$ ions produced into their lowest vibronic ground state by dissociative ionization and a mass selection 40 μs after ionization is expected to be very minor, as seen in Fig. 5 with the very receding threshold behavior of the $C_8H_6^+$ signal. This explains the reduction of the reaction cross section of m/z 141 and the non-detection of the channels m/z 116 and 129.

The latter reasoning can also be invoked to explain the apparent discrepancy between the present results and the conclusion from the group of Schwarz and co-workers,[23] who derived an absence (or at max 10%) of **PA**⁺ produced from dissociative ionization of **Naph**. The decisive method that leads to their conclusion is the double charge inversion +CR – where a high velocity collision with O_2 leads to the production of anion fragments provided they have a sufficient electron affinity. The formation of $C_8H_5^-$ was thus used as a proxy of the formation of **PA**⁺, as it was the main channel observed when $C_8H_6^+$ ions were produced by direct ionization from **PA** precursor. Since at most 10% of total signal was within the $C_8H_5^-$ channel when $C_8H_6^+$ ions were produced by dissociative ionization from **Naph** precursor, the formation of **PA**⁺ was considered as negligible. Yet, the 90% reduction in signal might have a similar origin as

the one observed for the *m/z* 141 channel in our experiment: a high sensitivity dependence to energy. Their apparatus allows similar timescale (maximum of 30 μs compared with 40 μs for us) for $C_8H_6^+$ ions to rearrange before to be probed. The difference in the outcome of the isomeric population compared with our experimental findings can thus be primarily imputed to the much larger amount of energy that they initially deposited into the $C_{10}H_8$ system.

Another experimental finding that, at first sight, is contradictory with our results comes from the work of Bouwman *et al.*[27] An infrared spectrum of the $C_8H_6^+$ fragments resulting from the dissociative ionization of **Naph** after multi photon excitation at 193 nm indicates unambiguously that the main structure formed is **PE**[+]. This conclusion is conflicting with ours. However, no power dependency studies were conducted to ensure that the ionization process was restricted to only two photons. Hence, two 193 nm photons correspond to an energy of ≈ 12.8 eV, barely above the thermodynamic dissociation threshold, and should mainly lead to **PA**[+], but three or four photons will bring 5 to 11 eV above the IE of **PA**, a region where **PE**[+] is the major structure of $C_8H_6^+$ ions according to Fig. 16 from ref. 25. Another experimental factor that plays a role in these conflicting results is the timescale of the experiment. Indeed, in Bouwman *et al.* experiment, the time given to the ions to explore the PES is extremely long (200 ms, with buffer gas (He) pressure of 2×10^{-5} mbar), so that if thermodynamically accessible, the most stable isomer, *e.g.* **PE**[+] should be formed.

The conclusions drawn by the work of Leach and coworkers using an experimental setup with a similar timescale as ours (a few tens of μs) were primarily based on the available heats of formation in the literature at that time for **PA**[+], **PE**[+], and one acyclic structure. They assumed that the most stable cation would be the preferred structure formed upon dissociation, which at that time was **PA**[+].[14,15] In the experimental studies performed by the Lifshitz group, they fit the dissociation curves as a function of time based on RRKM calculations. They first used the energy associated with the dissociation limit to **PA**[+] + C_2H_2,[17] and then to **BCB**[+] + C_2H_2,[21] once this structure was calculated to be more stable.[19,22] It seems that the experimental data against which the RRKM calculations were fit did not have the resolution to differentiate between the close-lying dissociation limits of the three main $C_8H_6^+$ isomers.

Conclusion

Recent theoretical studies converge on **PA**[+] as the main isomer resulting from the loss of acetylene from the $C_{10}H_8^+$ ions with less than 5.2 eV internal energy, whereas the results of experimental studies are more scattered. The origin of these experimental discrepancies can be twofold: (i) the way to generate $C_8H_6^+$ from $C_{10}H_8^+$ was different (electron ionization, one-photon dissociation, multi-photon dissociation) and (ii) the time integral for the chain of unimolecular reactions to proceed was very different. These two factors can greatly influence the isomeric distribution obtained. We found that **PA**[+] is the only isomer formed from single VUV photon dissociative ionization from **Naph** and **Azu** at least up to 4.7 eV above the $C_8H_6^+$ AEs within 40

μs. This is based on the exact same behavior of the reactivity leading to the product *m/z* 115 in region 1, 2, and 3 from **PA** with the results from **Naph** and **Azu**. The apparent underestimation of the branching ratio **PE**[+]/**PA**[+] up to 4.7 eV above the AE of **Naph** and **Azu** in our experiment compared with Dyakov *et al.*'s calculations[25] (215 kcal mol^{-1} in Fig. 16 of their paper) lies in the fact that the two cannot be directly compared. The calculations assume that the equilibrium is reached and that all the ion population has a unique internal energy, but in our experiment there is a kinetic restriction and all ions are produced with a distribution of internal energy based on Franck–Condon considerations.

This study has highlighted several crucial factors that should be consistently taken into account when comparing experimental studies conducted with varying apparatus and theoretical investigations:

- Consideration of measurement times and RRKM times.
- Consideration of the amount of internal energy depending on the ionization method, multiphoton absorption and their impact on reactivity and spectroscopic observables.
- Recognition of stimulated or assisted reactivity within reaction complexes, which can reveal ion structures kinetically absent when the object is isolated.

As VUV photon are ubiquitous in space, the present finding highlights the importance of **PA**[+] into the interstellar chemical network. The complementary study starting from **PA** also informed on the kinetics of the C_2H_2 elimination to form **PA**[+] from **Naph**[+] and **Azu**[+]. It was observed that **PA**[+] conserves all the energy put in the $C_{10}H_8$ systems, leaving the ejected C_2H_2 unit with nearly no internal or kinetic energy. We believe that this study sheds new light on the imbroglio concerning the $C_8H_6^+$ structures from dissociation of **Naph**[+] and **Azu**[+]. Furthermore, it also paves the way to challenging experiments where single and well-defined internal energy ions are generated by coincidence. Such experiments will allow direct comparisons with kinetic calculations restricted to 40 μs and should therefore end this imbroglio.

Data availability

The data that support the findings of this study are available from the corresponding author upon reasonable request.

Author contributions

U. J. conceived the project. U. J., C. Rossi, R. T., C. R., and C. A. performed the experiments and collected the data. R. T. and C. Rossi performed the data processing. C. Rossi generated the figures. U. J. wrote the manuscript. G. M. calculated the PES. P. M. and S. G. performed the RRKM and the MREP calculations. All authors discussed the results and commented on the manuscript.

Conflicts of interest

There are no conflicts to declare.

Acknowledgements

References

1 A. Léger and J. L. Puget, *Astron. Astrophys.*, 1984, **137**, 5–8.

2 L. Allamandola, A. Tielens and J. Barker, *Astrophys. J., Suppl. Ser.*, 1989, **71**, 733–775.

3 H. Richter, S. Granata, W. H. Green and J. B. Howard, *Proc. Combust. Inst.*, 2005, **30**, 1397–1405.

4 C. S. McEnally, L. D. Pfefferle, B. Atakan and K. Kohse-Höinghaus, *Prog. Energy Combust. Sci.*, 2006, **32**, 247–294.

5 A. G. Tielens, *Annu. Rev. Astron. Astrophys.*, 2008, **46**, 289–337.

6 Y. Wang, A. Raj and S. H. Chung, *Combust. Flame*, 2013, **160**, 1667–1676.

7 M. López-Puertas, B. M. Dinelli, A. Adriani, B. Funke, M. García-Comas, M. Moriconi, E. D'Aversa, C. Boersma and L. J. Allamandola, *Astrophys. J.*, 2013, **770**, 132.

8 L. Zhao, R. Kaiser, W. Lu, B. Xu, M. Ahmed, A. N. Morozov, A. M. Mebel, A. H. Howlader and S. F. Wnuk, *Nat. Commun.*, 2019, **10**, 1–7.

9 B. West, S. R. Castillo, A. Sit, S. Mohamad, B. Lowe, C. Joblin, A. Bodi and P. M. Mayer, *Phys. Chem. Chem. Phys.*, 2018, **20**, 7195–7205.

10 J. Zhen, P. Castellanos, D. M. Paardekooper, H. Linnartz and A. G. Tielens, *Astrophys. J., Lett.*, 2014, **797**, L30.

11 O. Berné, J. Montillaud and C. Joblin, *Astron. Astrophys.*, 2015, **577**, A133.

12 H. R. Hrodmarsson, J. Bouwman, A. G. Tielens and H. Linnartz, *Int. J. Mass Spectrom.*, 2022, 116834.

13 E. Ruehl, S. D. Price and S. Leach, *J. Phys. Chem.*, 1989, **93**, 6312–6321.

14 H. Jochims, H. Rasekh, E. Rühl, H. Baumgärtel and S. Leach, *Chem. Phys.*, 1992, **168**, 159–184.

15 H. Jochims, H. Rasekh, E. Rühl, H. Baumgärtel and S. Leach, *J. Phys. Chem.*, 1993, **97**, 1312–1317.

16 H. Jochims, E. Ruhl, H. Baumgartel, S. Tobita and S. Leach, *Astrophys. J.*, 1994, **420**, 307–317.

17 Y. Gotkis, M. Oleinikova, M. Naor and C. Lifshitz, *J. Phys. Chem.*, 1993, **97**, 12282–12290.

18 Y.-P. Ho, R. C. Dunbar and C. Lifshitz, *J. Am. Chem. Soc.*, 1995, **117**, 6504–6508.

19 Y. Ling, J. M. Martin and C. Lifshitz, *J. Phys. Chem. A*, 1997, **101**, 219–226.

20 G. Koster, J. M. Martin and C. Lifshitz, *J. Chem. Soc., Perkin Trans. 2*, 1999, 2383–2387.

21 W. Cui, B. Hadas, B. Cao and C. Lifshitz, *J. Phys. Chem. A*, 2000, **104**, 6339–6344.

22 G. Granucci, Y. Ellinger and P. Boissel, *Chem. Phys.*, 1995, **191**, 165–175.

23 K. Schroeter, D. Schröder and H. Schwarz, *J. Phys. Chem. A*, 1999, **103**, 4174–4181.

24 W. Van der Hart, *Int. J. Mass Spectrom.*, 2002, **214**, 269–275.

25 Y. A. Dyakov, C.-K. Ni, S. Lin, Y. Lee and A. Mebel, *Phys. Chem. Chem. Phys.*, 2006, **8**, 1404–1415.

26 E. A. Solano and P. M. Mayer, *J. Chem. Phys.*, 2015, **143**, 104305.

27 J. Bouwman, A. J. de Haas and J. Oomens, *ChemComm*, 2016, **52**, 2636–2638.

28 A. J. de Haas, J. Oomens and J. Bouwman, *Phys. Chem. Chem. Phys.*, 2017, **19**, 2974–2980.

29 B. J. West, L. Lesniak and P. M. Mayer, *J. Phys. Chem. A*, 2019, **123**, 3569–3574.

30 J. W. Lee, M. H. Stockett, E. K. Ashworth, J. E. Navarro Navarrete, E. Gougoula, D. Garg, M. Ji, B. Zhu, S. Indrajith, H. Zettergren, *et al.*, *J. Chem. Phys.*, 2023, **158**, 174305.

31 C. Rossi, C. Alcaraz, R. Thissen and U. Jacovella, *J. Phys. Org. Chem.*, 2023, e4489.

32 U. Jacovella, C. Rossi, C. Romanzin, C. Alcaraz and R. Thissen, *ChemPhysChem*, 2022, **23**, e202100871.

33 U. Jacovella, C. Rossi, C. Romanzin, C. Alcaraz and R. Thissen, *ChemPhysChem*, 2023, **24**, e202200474.

34 L. Nahon, N. de Oliveira, G. A. Garcia, J.-F. Gil, B. Pilette, O. Marcouillé, B. Lagarde and F. Polack, *J. Synchrotron Radiat.*, 2012, **19**, 508–520.

35 B. Cunha de Miranda, C. Romanzin, S. Chefdeville, V. Vuitton, J. Žabka, M. Polášek and C. Alcaraz, *J. Phys. Chem. A*, 2015, **119**, 6082–6098.

36 M. J. Frisch, G. W. Trucks, H. B. Schlegel, G. E. Scuseria, M. A. Robb, J. R. Cheeseman, G. Scalmani, V. Barone, G. A. Petersson, H. Nakatsuji, X. Li, M. Caricato, A. V. Marenich, J. Bloino, B. G. Janesko, R. Gomperts, B. Mennucci, H. P. Hratchian, J. V. Ortiz, A. F. Izmaylov, J. L. Sonnenberg, D. Williams-Young, F. Ding, F. Lipparini, F. Egidi, J. Goings, B. Peng, A. Petrone, T. Henderson, D. Ranasinghe, V. G. Zakrzewski, J. Gao, N. Rega, G. Zheng, W. Liang, M. Hada, M. Ehara, K. Toyota, R. Fukuda, J. Hasegawa, M. Ishida, T. Nakajima, Y. Honda, O. Kitao, H. Nakai, T. Vreven, K. Throssell, J. A. Montgomery Jr., J. E. Peralta, F. Ogliaro, M. J. Bearpark, J. J. Heyd, E. N. Brothers, K. N. Kudin, V. N. Staroverov, T. A. Keith, R. Kobayashi, J. Normand, K. Raghavachari, A. P. Rendell, J. C. Burant, S. S. Iyengar, J. Tomasi, M. Cossi, J. M. Millam, M. Klene, C. Adamo, R. Cammi, J. W. Ochterski, R. L. Martin, K. Morokuma, O. Farkas, J. B. Foresman and D. J. Fox, *Gaussian 16 Revision C.01*, Gaussian Inc, Wallingford CT, 2016.

37 T. Baer and W. L. Hase, *Unimolecular reaction dynamics: theory and experiments*, Oxford University Press on Demand, 1996, vol. 31.

38 T. Beyer and D. Swinehart, *Commun. ACM*, 1973, **16**, 379.

39 T. Baer and P. M. Mayer, *J. Am. Soc. Mass Spectrom.*, 1997, **8**, 103–115.

40 J. Dyke, H. Ozeki, M. Takahashi, M. Cockett and K. Kimura, *J. Chem. Phys.*, 1992, **97**, 8926–8933.

41 U. Jacovella, C. Rossi, C. Romanzin, C. Alcaraz and R. Thissen, *ChemPhysChem*, 2022, **23**, e202100871.

42 J. Maier and D. Turner, *J. Chem. Soc., Faraday Trans.*, 1973, **69**, 521–531.

43 T. Baer, O. Dutuit, H. Mestdagh and C. Rolando, *J. Phys. Chem.*, 1988, **92**, 5674–5679.